6ICEGE 6th International Conference on Earthquake Geotechnical Engineering
1-4 November 2015
Christchurch. New Zealand

Effect of Pore Pressure on Seismic Soil Response: 1D-3 Components Numerical Modelling

V.A. Pham[1], F Bonilla[2], L. Lenti[3], J-F Semblat[4]

ABSTRACT

During strong quakes, the propagation of seismic waves in soil layers involves nonlinearities changing with the excitation level. Furthermore, the influence of the pore pressure cannot be neglected for saturated soils. Starting from a FEM formulation describing 1D propagation and three-dimensional loading ("1D- 3 components approach"), the influence of the fluid is accounted for through a relation between the pore pressure and the work of the three-dimensional stress state initially proposed by Iai. It has been validated through comparisons to laboratory tests. Three-components synthetic motions have also been considered and the results are satisfactory both in terms of accelerations as well as pore pressure build-up. Ongoing researches investigate the seismic response of realistic soil columns during 4 actual quakes (Superstition Hills, 1987, USA, Mw=6.7; Tohoku, 2011, Japan, Mw=9.1; Kushiro, 1993, Japan, Mw=7.8; Emilia, 2012, Italy, Mw=5.9).

Introduction

The soil response to strong seismic excitations should account for the time variations of the stresses and strains. Various one-dimensional models have been proposed in previous researches (Joyner and Chen, 1975; Pyke, 1979; Bonilla, 2000; Hartzell et al., 2004; Phillips and Hashash, 2009; Segalman and Starr, 2008; Delépine et al., 2009). The rheological description often raises the need for tens of parameters difficult to estimate in large sedimentary basins.

The nonlinear constitutive law proposed in this paper (Santisi et al., 2012) is based on the definition of several plasticity surfaces involving a limited number of parameters that could be estimated from simple laboratory tests (shear modulus reduction for dry soils, determination of a “liquefaction front” for saturated soils).

In particular, the role of water is accounted for through a “liquefaction front” approach initially proposed by Towhata & Ishihara (1985) and Iai et al. (1990a,b). This model is based on the identification of an empirical relationship between the pore pressure and the work of the shear stress derived from laboratory tests (Bonilla, 2000).

[1]Dr, Dept GERS, IFSTTAR, 14-20 bd Newton, Champs sur Marne, France, viet-anh.pham@ifsttar.fr
[2]Dr, Dept GERS, IFSTTAR, 14-20 bd Newton, Champs sur Marne, France, fabian.bonilla@ifsttar.fr
[3]Dr, Dept GERS, IFSTTAR, 14-20 bd Newton, Champs sur Marne, France, luca.lenti@ifsttar.fr
[4]Dr, Dept GERS, IFSTTAR, 14-20 bd Newton, Champs sur Marne, France, jean-francois.semblat@ifsttar.fr

This constitutive law for saturated soils has been implemented in a finite element code in order to estimate the seismic response of a 1D soil profile accounting for the simultaneous propagation of the three components of the seismic motion. The influence of the pore pressure will thus be analysed through the comparison of various examples.

Modeling 3C Seismic Wave Propagation

The three motion components are propagated vertically in a multilayered soil profile (Figure 1). The soil profile includes several homogeneous horizontal layers (*xy* plane) with various thicknesses. The layered soil is discretized through quadratic 3 noded elements. Since the full 3C polarization is considered, both pressure and shear waves are propagated along the *z* direction.

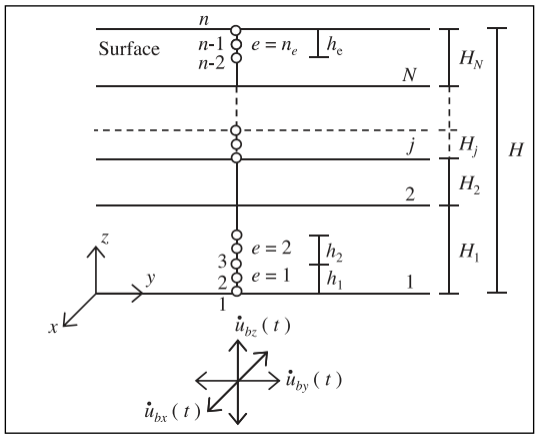

Figure 1. Spatial discretization of the horizontally multilayered soil.

The weak formulation of the equation of motion for a soil column considering a nonlinear constitutive law and a spatial discretization may be written as follows:

$$[\mathrm{M}]\{\ddot{\mathrm{D}}\} + [\mathrm{C}]\{\dot{\mathrm{D}}\} + \{\mathrm{F_{int}}\} = \{\mathrm{F}\} \tag{1}$$

In Equation (1), $[M]$ is the mass matrix; $\{\dot{\mathrm{D}}\}$ and $\{\ddot{\mathrm{D}}\}$ are the first and second time derivatives of the displacement vector $\{D\}$ respectively; $\{F_{int}\}$ is the vector of internal forces and $\{\mathrm{F}\}$ is the vector of external loadings; $[C]$ being a matrix depending on the boundary conditions.

The system of horizontal soil layers is bounded at top ($z=H$) by a free surface and at the bottom by the bedrock with elastic boundary conditions considering a prescribed displacement u_b. The equation of motion may be more conveniently expressed considering the relative displacements $\{X\}$ with respect to the base of the soil column:

$$\{\mathrm{X}\} = \{\mathrm{D}\} - \{\mathrm{I}\}\mathrm{u_b} \tag{2}$$

Equation (1) then becomes:

$$[\mathrm{M}]\{\ddot{\mathrm{X}}\} + [\mathrm{K}]\{\mathrm{X}\} = -[\mathrm{M}]\{\mathrm{I}\}\ddot{\mathrm{u}}_\mathrm{b} \tag{3}$$

The vector $\{I\}$ is a unit column matrix and $[K]$ is the tangent stiffness matrix. The nonlinear behaviour leads to a time-varying matrix $[K]$. We consider Newmark algorithm to solve Equation (2) in the time domain (displacements increments are denoted $\{\Delta X\}$). This method is detailed in Santisi et al. (2012).

Proposed Constitutive Law

To model three-components wave propagation in layered soils, we need a 3D constitutive law. In this work, the proposed approch combines two different models: a nonlinear constitutive law for the soil with a three-dimensional stress state (MPii model, Iwan (1967), Segalman and Starr (2008)) and a model accounting for the dependency of the pore pressure on the work of the shear stress proposed by Iai et al. (1990a,b). Iwan's model is first considered to compute the total stresses. Then, through Iai's model, the total stresses are corrected to estimate the effective stresses by evaluating the shear work on a given soil volume at each time step and using the empirical relations making the link with the pore pressure.

Constitutive Law for Dry Soil

The MPii model (Iwan, 1967; Joyner et Chen, 1975; Joyner, 1975; Santisi et al, 2012; Segalman and Starr, 2008) accounts for the nonlinear hysteretic behaviour of the soil considering a hardening elastic-plastic approach through a series of plasticity surfaces.

For a one-dimensional model, one considers a series of rheological cells combining a linear spring and a friction unit (Figure 2). The friction unit *i* remains locked until the stress reaches the value Y_i. The spring constants, G_i, are chosen in order to recover the stress-strain behaviour observed in the laboratory.

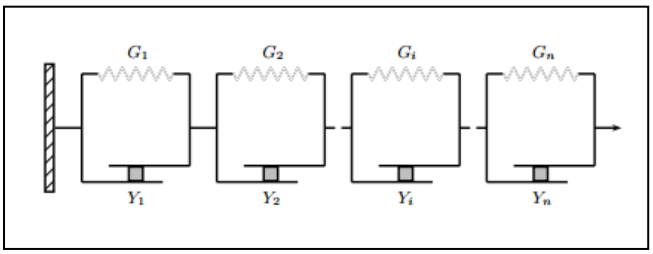

Figure 2. 1D rheological model originally proposed by Iwan (1967).

For a three-dimensional problem, Iwan (1967) extended the classical theory of incremental plasticity (Fung, 1965). Instead of a single plasticity surface, we consider a family of plasticity surfaces. The 3D stress-strain "MPii" relation may then be expressed as (Santisi et al., 2012):

$$\{\Delta\sigma\} = [\mathrm{E}]\{\Delta\varepsilon\} \tag{4}$$

$$\{\Delta\varepsilon\} = \{\Delta\varepsilon_{xx}\ \ \Delta\varepsilon_{yy}\ \ \Delta\gamma_{xy}/2\ \ \Delta\gamma_{yz}/2\ \ \Delta\gamma_{zx}/2\ \ \Delta\varepsilon_{zz}\}^{\mathrm{T}} \tag{5}$$

$$\{\Delta\sigma\} = \{\Delta\sigma_{xx}\ \ \Delta\sigma_{yy}\ \ \Delta\tau_{xy}\ \ \Delta\tau_{yz}\ \ \Delta\tau_{zx}\ \ \Delta\sigma_{zz}\}^{\mathrm{T}} \tag{6}$$

where $[E]$ is the total constitutive matrix given by the MPii model. This matrix allows the evaluation of the stress increment $\{\Delta\sigma\}$ from the strain increment $\{\Delta\varepsilon\}$.

3D Liquefaction Front Model for Saturated Soils

The liquefaction front model is an empirical approach to describe the reduction of the effective mean stress due to the increase in the pore pressure. This approach allows to simulate the liquefaction and cyclic mobility of sands. It is based on correlations between the shear work and the pore pressure obtained by Towhata and Ishihara (1985). The equations for the liquefaction approach were derived by Iai et al. (1990a,b) and the concept is briefly explained hereafter.

In the 2D case, the correlation between the effective stress and the shear stress is displayed in Figure 3. When the effective stress decreases, the shear stress gets closer to the failure line. There are two different limits: the phase transformation line (where dilatancy starts), and the failure line (where liquefaction occurs). These two lines are respectively characterized by the phase transformation angle φ_P and the friction angle φ.

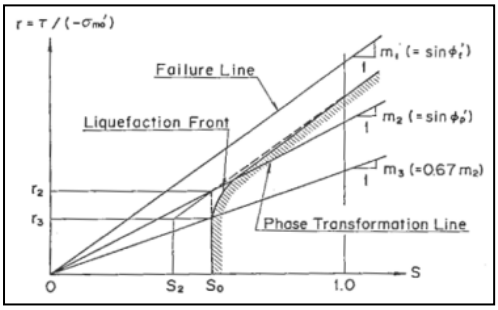

Figure 3. Principle of the liquefaction front approach in the S − r plane.

In this work, we extend the model to three dimensions and the liquefaction front will be characterized by the state variable S and the ratio r. The state variable $S = p'/p'_0$ is the ratio between the current effective mean stress p' and the initial effective mean stress p'_0; it ranges from 1 (no pore pressure build-up) to 0 (liquefaction). The ratio of the deviatoric stresses $r = q/p'_0$ is the ratio between the deviatoric stress q and the initial effective mean stress p'_0: $p'_0 = (\sigma'_{0xx}+\sigma'_{0yy}+\sigma'_{0zz})/3$. The relationship between parameters *S* and *r* in three dimensions (3D) is similar to that in two dimensions (2D) considering the following parameters:

$$S = \begin{cases} S_0 & \text{if } r < r_3 \\ S_2 + \sqrt{(S_0 - S_2)^2 + [(r - r_3)/m_1]^2} & \text{if } r > r_3 \end{cases} \quad (7)$$

where: $S_2 = S_0 - (r_2 - r_3)/m_1$; $r_2 = m_2 S_0$; $r_3 = m_3 S_0$; $m_1 = \sin\varphi$□; $m_2 = \sin\varphi_P$ and $m_3 = 0.67 m_2$. S_0 is a parameter defined as a function of the shear work; $m_1 = \sin\varphi$ is the slope of the failure line; $m_2 = \sin\varphi_P$ is the slope of the phase transformation line.

Parameter S_0 is called the 'liquefaction front parameter' and may be interpreted as a measure of the liquefaction level. The 'liquefaction front parameter' S_0 is given through a function of the shear work as described by Iai et al. (1990a,b).

It reads:

$$S_0 = \begin{cases} 1 - 0.6\left(\frac{w}{w_1}\right)^{p_1} & \text{if } w < w_1 \\ (0.4 - S_1)\left(\frac{w_1}{w}\right)^{p_2} + S_1 & \text{if } w > w_1 \end{cases} \quad (8)$$

where S_1, w_1, p_1, p_2 are parameters characterizing the evolution of the pore pressure towards liquefaction or cyclic mobility of sands. There are estimated from undrained cyclic laboratory tests.

Validation of the MPii-L Model

Validation in Undrained Cyclic Deformation

In this type of test, the cyclic loading with controlled constant shear strain amplitude is applied and the shear stress is recorded. The tests were performed by Zaheer et al. (2012). For all tests, the standard sinusoidal displacement wave was applied at frequency of 0.1Hz. The soil taken for this test is Leighton Buzzard EFraction sand. This dense sand prepared with initial relative density of 80% with corresponding void ratio of 0.72 and tested at the initial vertical effective stress of 250 kPa. Figs. 4 and 5 display the predicted (MPii-L simulation) and measured (laboratory test) stress-strain and pore pressure response for dense samples. The results in terms of stress-strain and pore pressure response of the numerical simulation predict reasonably well the experimental results.

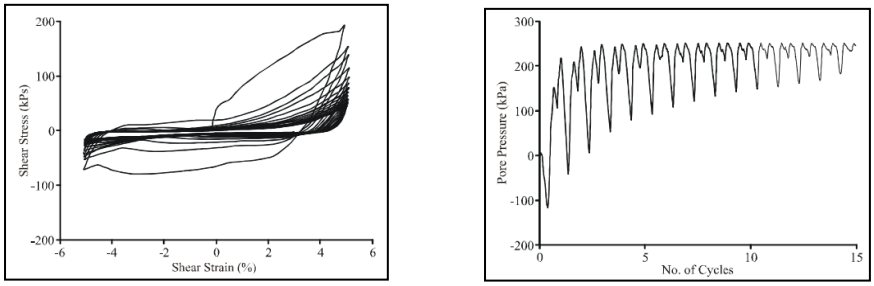

Figure 4: Stress-strain path and pore pressure curve for dense sand obtained experimentally at a strain amplitude of 5% (after ZAHEER, 2012)

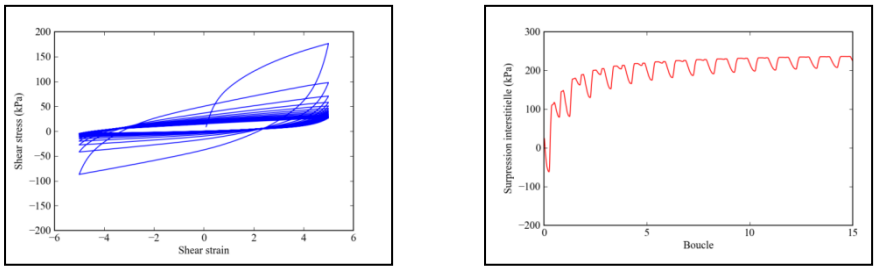

Figure 5: Stress-strain path and pore pressure curve obtained numerically (MPii-L model) at a strain amplitude of 5%

Multidirectional Influences

This model can be generalized to any three-dimensional stress and tested on real cases. In this context, this MPii-L model will be analyzed in the simple real case, the propagation of seismic waves in the vertical direction z. The assumption on geometry imposes zero strain variations in the directions x and y. This is to say that there are still three components imposed deformations. These are ε_{xz}, ε_{yz}, ε_{zz}. In this section, the results of the simulation is analyzed in the case of three simultaneously imposed to express the influence of the polarization of the wave components. In this simulation, all three components are applied simultaneously on an element. The results are compared to results obtained with a single strain component. Three strain components are considered through the following ratios:

$$\begin{cases} \varepsilon_{yz} = \eta_1 \varepsilon_{xz} \\ \varepsilon_{zz} = \eta_2 \varepsilon_{xz} \end{cases} \tag{9}$$

where η_1, η_2 are the ratios of shear strain ε_{yz} and axial strain ε_{zz} with respect to shear strain ε_{xz}. In the section, the values of η_1, η_2 are 0.5 and 0.1, respectively. The shear strain component ε_{xz} is the largest component. All three components are displayed in Figure 6.

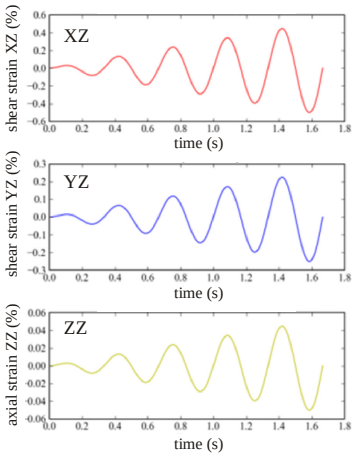

Figure 6: Imposed three components: shear strain xz (black curve), shear strain yz (blue curve), axial strain zz (yellow curve)

Figure 7(a,b,c,d) shows the comparison between the three prescribed components and the single prescribed component. In the case of three prescribed components, the results consist of four red curves. These are respectively the stress - strain relationships $\varepsilon_{xz} - \sigma_{xz}$, $\varepsilon_{yz} - \sigma_{yz}$, $\varepsilon_{zz} - \sigma_{zz}$ and pore pressure versus time. In the case of a single component, the three curves correspond to three single prescribed strains: ε_{xz}, ε_{yz}, ε_{zz}. For each case, the results are shown by two curves, the stress-strain curve and the pore pressure versus time. Comparing the stress-strain relationships, the influence of the largest stress component leads to a decrease of the shear stresses obtained for three prescribed components when compared to the case of the single prescribed component. The decrease of σ_{zz} for three prescribed components with respect to one single component is not significant.

We also note that the pore pressure obtained for three prescribed components is different from that obtained for a single prescribed component ε_{yz}, ε_{zz}, and almost identical to the pore pressure obtained for a single prescribed strain ε_{xz}. This shows the influence of the various components and the effect of the largest component. The stresses obtained for three prescribed components are smaller than the stresses obtained for a single component. From Figure 7(e,f), this is obvious when plotting the octahedral stress (Santisi et al., 2012):

$$\tau_{octa} = \frac{1}{3}\sqrt{\left(\sigma_{xx}-\sigma_{yy}\right)^2+\left(\sigma_{yy}-\sigma_{zz}\right)^2+\left(\sigma_{zz}-\sigma_{xx}\right)^2+6\left(\tau_{xy}^2+\tau_{yz}^2+\tau_{xz}^2\right)} \quad (10)$$

with respect to the octahedral shear strain:

$$\gamma_{octa} = \frac{2}{3}\sqrt{2\varepsilon_{zz}^2+6\left(\varepsilon_{xz}^2+\varepsilon_{yz}^2\right)} \quad (11)$$

In Figure 7(e), the octahedral stress is plotted with respect to the octahedral strain. We can notice that in both cases (three or one prescribed component(s)), there is a decrease in the shear octahedral modulus G_{octa}. In Figure 7(f), the octahedral stress for three prescribed components appears to be much smaller than that for a single prescribed component. As already shown by Santisi et al. (2012), this stress decrease is due to the influence of the 3D stress path on the nonlinear soil response.

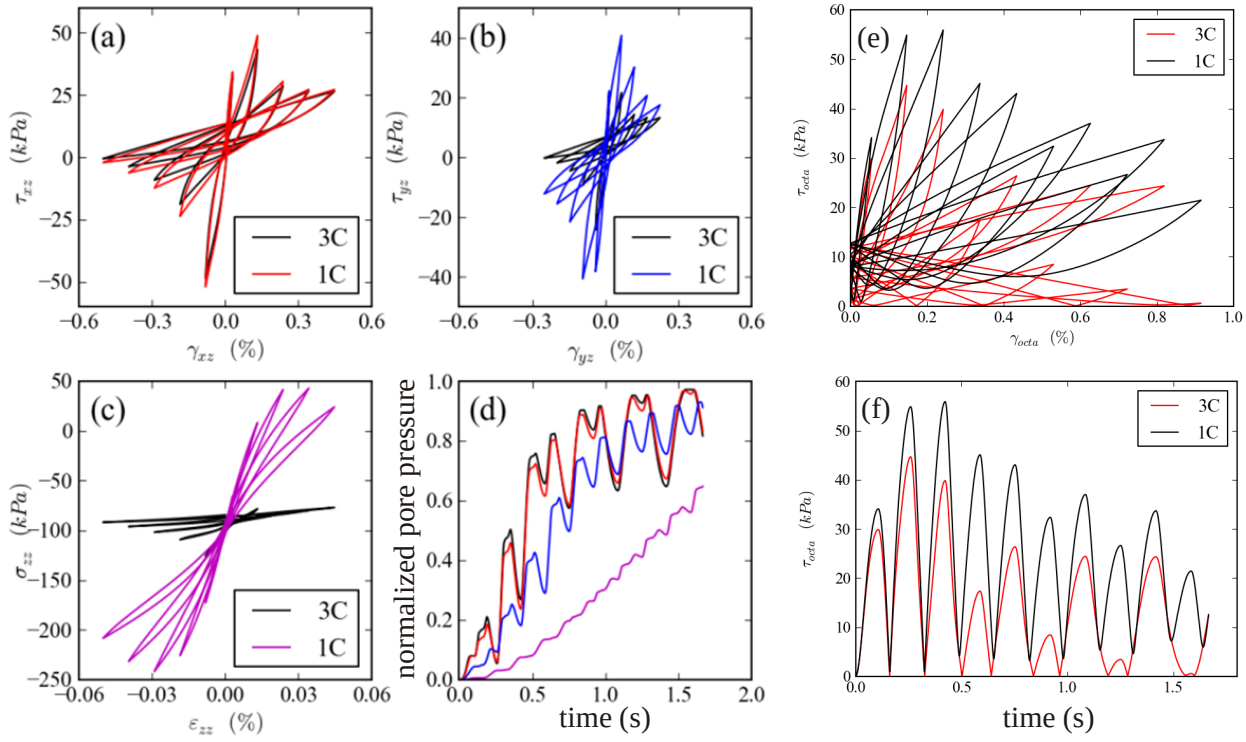

Figure 7: Effect of polarization, comparison between three and one prescribed component(s): a) component ε_{xz}; b) ε_{yz} component; c) component ε_{zz}; d) pore pressure; e,f) octahedral stress.

Conclusion

The combination of the MPii model and the "liquefaction front approach" allows a realistic modeling of the cyclic response of saturated soils. This model has been derived in 3 dimensions thus allowing the analysis of the influence of the largest stress and strain component on the cycli response of saturated soils loaded by a full 3C seismic wave. In this paper, the differences between the stress-strain and pore pressure curves obtained for three or one prescribed component(s) are significant. Ongoing researches investigate the seismic response of actual soil columns during the Tohoku (Japan) and Emilia (Italy) earthquakes for which important liquefaction phenomena have been reported.

References

Bonilla LF. 2000. *Computation of linear and nonlinear site response for near field ground motion*, PhD, University of California, Santa Barbara.

Delépine N., Bonnet G., Lenti L., Semblat J.F., 2009. Nonlinear viscoelastic wave propagation: an extension of Nearly Constant Attenuation models, *J Eng Mech*, **135**(11): 1305-1314.

Fung YC. 1965. *Foundation of Solid Mechanics*, Prentice Hall, Englewood Cliffs, NJ.

Hartzell S, Bonilla LF, Williams RA. Prediction of nonlinear soil effects, *Bull. Seism. Soc. Am*. 2004; **94**(5): 1609-1629.

Iai S, Matsunaga Y, Kameoka T. Strain space plasticity model for cyclic mobility, *Report of the Port and Harbour Research Institute* 1990a.; **29**(4): 27-56.

Iai S, Matsunaga Y, Kameoka T. Parameter identification for cyclic mobility model, *Report of the Port and Harbour Research Institute* 1990b; **29**(4): 57-83.

Iwan WD. On a class of models for the yielding behaviour of continuous and composite systems, *Journal of Applied Mechanics* 1967; **34**(E3): 612-617.

Joyner W. A method for calculating nonlinear seismic response in two dimensions, *Bull. Seism. Soc. Am*. 1975. **65**(5): 1337-1358.

Joyner WB, Chen ATF. Calculation of nonlinear ground response in earthquakes, *Bull. Seism. Soc. Am*. 1975, **65**(5): 1315-1336.

Masing G.. Eigenspannungen und Verfertigung beim Messing, *2nd International Congress on Applied Mechanics*, Zurich, Switzerland, 1926; 332-335.

Phillips C, Hashash YMA. Damping formulation for nonlinear 1D site response analyses, *Soil Dyn. Earthq. Eng*. 2009; **29**(7): 1143-1158.

Pyke R, Nonlinear model for irregular cyclic loadings, J. Geotech. Eng. Div. 1979; **105**:715–726.

Santisi d'Avila MP, Lenti L, Semblat JF. Modelling strong seismic ground motion: three-dimensional loading path versus wavefield polarization, *Geophysical Journal International* 2012; **190**(3): 1607-1624.

Segalman DJ, Starr MJ. Inversion of Masing models via continuous Iwan systems, *Int. J. Nonlinear Mech*. 2008; **43**: 74-80.

Towhata I, Ishihara K. Modelling of soil behaviour under principal stress axis rotation, *5th International Conference on Numerical Methods in Geomechanics*, Nagoya, 1985; **1**: 523-530.